Evolution of an Ensemble of Nanoparticles in a Colloidal Solution: Theoretical Study

Dmitri V. Talapin,*,† Andrey L. Rogach,† Markus Haase, and Horst Weller

Institute of Physical Chemistry, University of Hamburg, 20146 Hamburg, Germany

Received: June 13, 2001; In Final Form: July 28, 2001

The evolution of a nanosized particle in colloidal solution has been studied theoretically. The model developed is based on the size dependence of the activation energies of the growth and dissolution processes and takes into account the mass transport dynamics. Using this model, Monte Carlo simulations of the evolution of an ensemble of growing nanoparticles during Ostwald ripening have been performed, and conditions leading to either "focusing" or "defocusing" of the particle size distribution were found. The stationary particle size distribution inherent to the Ostwald ripening process in ensembles of nanoparticles less than 5 nm in radius is narrower and more symmetric than that predicted by the Lifshitz−Slyozov−Wagner theory valid for ensembles of larger (>20 nm in radius) colloidal particles. The growth of nanoparticles in the diffusion-controlled regime results in better final size distributions as compared with those grown in the reaction-controlled regime. The dependence of the particle size distribution on a number of external and internal ensemble characteristics is studied and possible ways of controlling the particle size distribution are discussed.

1. Introduction

Semiconductor nanoparticles (NPs), also called nanoclusters, nanocrystals, or chemically grown quantum dots, with particle sizes typically less than 10 nm have attracted much attention during last two decades.[1] Recent successful integration of luminescent CdSe, CdTe, and core−shell (e.g. CdSe/ZnS) NPs into light-emitting diodes[2−4] and their use as biological labels[5,6] make quantum dots interesting for commercial applications. A lot of work was devoted to the preparation of high quality II−VI and III−V semiconductor quantum dots[7−12] and investigation of their optical properties.[13−16] On the other hand, there is a lack of theoretical understanding of the processes occurring during the growth of NPs in colloidal solutions. Only a few reports deal with this important problem.[17,18] Peng et al. described the conditions when narrowing ("focusing") and broadening ("defocusing") of the particle size distribution occurs during the growth of several II−VI and III−V NPs.[17] The results were explained in the framework of a model developed by Sugimoto, describing the growth of a single colloidal particle at constant external surrounding and valid for micrometer-scale systems rather than nanometer-scale ones.[19] However, in the reaction vessel containing an ensemble of growing NPs at any instant of time a lot of colloidal particles compete for a finite amount of monomer, and the number of particles changes gradually due to the particle "birth" and "death" processes. Here and below, we use the term "ensemble" to describe the whole population of particles presented in the colloidal solution at different instants of time. The term "monomer" refers to any molecular precursor(s) participating in the reversible act of adding/removing a molecular unit (e.g., Cd or Se atoms) to a NP (e.g., CdSe) in the reaction vessel.

An important point of the dynamics of the ensemble evolution is the intrinsic polydispersity of colloidal particles, which can result in Ostwald ripening. Ostwald ripening is the growth mechanism where smaller particles dissolve and the monomer thereby released is consumed by the large ones.[20] Lifshitz and Slyozov[21] and Wagner[22] have developed an elegant asymptotic solution for the evolution of an ensemble of particles during Ostwald ripening (LSW theory). The appearance of the LSW approach has stimulated a lot of attempts to describe the Ostwald ripening analytically[23−26] and to verify the LSW and more recent theories experimentally.[27−30] Whereas in the stationary regime the competition of growing colloidal particles for the monomer can be treated analytically by the LSW theory, no general solution exists for the earlier transient stages of the particle growth.[24,31] Extensive numerical simulations of Ostwald ripening were performed therefore to treat self-consisted model of the particle ensemble evolution.[24,25,31−33] It was shown that for realistic initial size distributions the stationary regime was not attained even after an increase of the average particle radius by a factor of 4.[31]

Both theoretical and numerical simulations of Ostwald ripening fail to describe real ensembles of nanosized particles as they use only two terms of the expansion of the Gibbs−Thompson equation:

$$C(r) = C^0_{\mathrm{flat}} \exp\left[\frac{2\gamma V_{\mathrm{m}}}{rRT}\right] \approx C^0_{\mathrm{flat}}\left(1 + \frac{2\gamma V_{\mathrm{m}}}{rRT}\right) \qquad (1)$$

Here, C(r) and C^0_{flat} are the solubility of a particle with radius r and of the bulk material, respectively, γ is the surface tension, and V_{m} is the molar volume of the solid. The coefficient $2\gamma V_{\mathrm{m}}/(RT)$ called "capillary length" is usually of the order of 1 nm,[27,31] and eq 1 satisfactory describes the solubility of colloidal particles whose radius is larger than ca. 20 nm. For NPs with $r = 1-5$ nm the value of the capillary length is approaching the particle radius, and the particle solubility becomes strongly nonlinear against r^{-1}. Moreover, the chemical potential of nanoparticles and, as a result, the rate of the interface reactions also depend nonlinearly on r^{-1} as will be described below. Both effects were not taken into account in the classical description

* Corresponding author. Fax: +49-40-42838-3452. E-mail: talapin@chemie.uni-hamburg.de. WWW: http://www.chemie.uni-hamburg.de/pc/AKs/Weller/.

† On leave from Physico-Chemical Research Institute, Belarusian State University, 220050 Minsk, Belarus.

10.1021/jp012229m CCC: $20.00
Published on Web 11/15/2001

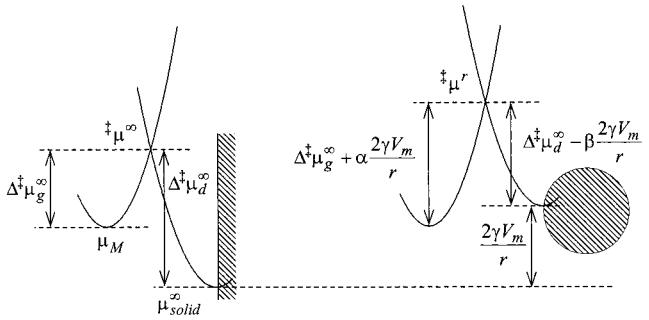

Figure 1. Schematic description of the size dependence of the activation energies for growth and dissolution processes.

of the reaction-controlled Ostwald ripening. Probably, the description of the ensemble taking into account the above-mentioned effects cannot be done analytically in the framework of the existing mathematical approaches.

In this paper we present a model allowing to calculate the size evolution of a NP under reaction, diffusion, and mixed reaction−diffusion control (Section 2). We have performed Monte Carlo simulations of Ostwald ripening of an ensemble of growing NPs (section 4.2.1.). The conditions leading to "focusing" and "defocusing" of the particle size distribution under mixed diffusion-reaction control have been investigated (section 4.2.2).

2. Evolution of a Single NP in a Colloidal Solution

We start with a model describing the behavior of a single NP of radius r placed in an infinite volume of solution with a constant concentration of monomer, thereafter referred to as the bulk concentration [M]. The monomer can react with the surface, thereby adding a new unit to the particle (NP grows) or can leave the surface, thereby removing one unit (NP dissolves). Both processes occur along the reaction path including the activated complex with the chemical potential $^{\ddagger}\mu$ (Figure 1). The resulting activation energies for growth and dissolution of the NP are $\Delta^{\ddagger}\mu_g$ and $\Delta^{\ddagger}\mu_d$, respectively. The chemical potential of the solid depends on the curvature of the surface by means of the Kelvin equation,[34] and the activation energy $\Delta^{\ddagger}\mu$ is a function of the particle radius:

$$\Delta^{\ddagger}\mu_g(r) = \Delta^{\ddagger}\mu_g^{\infty} + \alpha\frac{2\gamma V_m}{r} \tag{2}$$

$$\Delta^{\ddagger}\mu_d(r) = \Delta\mu_d^{\ddagger\infty} - \beta\frac{2\gamma V_m}{r} \tag{3}$$

where α and β are the transfer coefficients ($\alpha + \beta = 1$); $\Delta^{\ddagger}\mu^{\infty}$ is an activation energy in the case of the flat interface.

In the framework of the theory of the activated complex, the rate constant can be expressed through the height of the activation barrier:[34]

$$k = B\exp(-\Delta^{\ddagger}\mu/RT) \tag{4}$$

where B is a constant with the same dimension as k.

In the case of the polynuclear-layer growth mechanism,[35] which seems to be the most probable for NPs in colloidal solution, the flux of monomer J_g^{react} toward the particle surface is described by a first-order surface reaction:

$$J_g^{react} = 4\pi r^2 k_g[M]_r = 4\pi r^2 k_g^{flat}[M]_r \exp\left[-\alpha\frac{2\gamma V_m}{rRT}\right] \tag{5}$$

where $[M]_r$ is the concentration of the monomer near the particle surface and $k_g^{flat} = B_g\exp(-\Delta^{\ddagger}\mu_g^{\infty}/RT)$ is the growth rate constant for growth of a flat ($r = \infty$) surface.

In the simple case when the rate of the dissolution of a solid does not depend on the monomer concentration in solution, the flux of monomer J_d^{react} toward the particle surface can be expressed as follows:

$$J_d^{react} = -4\pi r^2 k_d = -4\pi k_d^{flat} r^2 \exp\left[\beta\frac{2\gamma V_m}{rRT}\right] \tag{6}$$

where $k_d^{flat} = B_d\exp(-\Delta^{\ddagger}\mu_d^{\infty}/RT)$ is the dissolution rate constant for a flat ($r = \infty$) interface.

The ratio between k_d^{flat} and k_g^{flat} gives the equilibrium constant for the dissolution of the bulk material $K_{eq} = a_{solute}/a_{solid} \approx C_0^{flat}$ (a is an activity of a component):

$$K_{eq} = k_d^{flat}/k_g^{flat} = C_0^{flat} \tag{7}$$

Diffusion of the monomer from the bulk of solution toward the particle surface is expressed by Fick's first law:

$$J^{diff} = 4\pi x^2 D\left(\frac{d[M]}{dx}\right)_{x\geq r} \tag{8}$$

where D is the diffusion coefficient and x is the distance from the center of the particle.

Integration of [M] from $r + \delta$ to r, where δ is the thickness of the diffusion layer, gives the steady-state flux toward an isolated spherical particle:[19,36]

$$J^{diff} = \frac{4\pi D r(r+\delta)}{\delta}([M]_{bulk} - [M]_r) \tag{9}$$

where $[M]_{bulk}$ is the monomer concentration in the bulk of solution and δ is the thickness of the diffusion layer.

As was mentioned by Peng et al.,[18] under real conditions the size of the NP is negligible compared to the thickness of diffusion layer ($r \ll \delta$) and eq 9 can be simplified:

$$J^{diff} = 4\pi D r([M]_{bulk} - [M]_r) \tag{10}$$

Note that, upon stirring of the solution, the diffusion coefficient has to be replaced by the mass-transfer coefficient which can be calculated or experimentally estimated for any particular case.

Under steady-state conditions the number of monomer units added and removed from the particle surface have to be equal to those diffusing toward the particle from the bulk of the solution. Hence,

$$J_g^{react} - J_d^{react} = J^{diff} \tag{11}$$

Substitution of eqs 5, 6, and 10 into eq 11 allows expressing the stationary concentration of the monomer near the particle interface:

$$[M]_r = \frac{D[M]_{bulk} + rk_d^{flat}\exp\left[\beta\frac{2\gamma V_m}{rRT}\right]}{rk_g^{flat}\exp\left[-\alpha\frac{2\gamma V_m}{rRT}\right] + D} \tag{12}$$

In the case of purely diffusion-controlled dissolution, the stationary concentration estimated from eq 12 tends to the equilibrium value described by eq 1.

TABLE 1: Values of Numerical Parameters Used in the Monte Carlo Simulations of NP Ensembles

parameter		value	comments
initial monomer oversaturation	S_0	1−1000	constant (15) in Figures 3−6
parameter describing the type of the control	K	10^{-3}−10^{3}	$K \ll 1$: diffusion-controlled process $K \gg 1$: reaction-controlled process
initial mean particle radius	$\langle r \rangle$	1.0 nm	
initial standard deviation of the particle size distribution	σ_0	5−35%	Normal distribution. Constant (20%) in Figures 3−5, 7−9
specific surface energy	γ	5×10^{-3}−1 J m^{-2}	constant (0.125 J m^{-2}) in Figures 3−5, 7−9
diffusion coefficient	D	10^{-12} m^2 s^{-1}	
simulated volume of the colloidal solution	V_{sln}	3×10^{-12} m^3	
number of simulated NPs	N	5×10^{3}−5×10^{4}	
solubility of the monomer in equilibrium with a flat interface	C^0_{flat}	10^{-2} mol m^{-3}	
molar volume	V_m	3.29×10^{-5} m^3	the value corresponds to wurtzite CdSe
transfer coefficients	α,β	0.5	
number of time steps		10^{4}−10^{5}	

Substitution of the stationary monomer concentration into eq 10 gives the expression for the total flux of monomers toward the particle surface. On the other hand, J is related to the particle growth rate dr/dt as[19]

$$J = (4\pi r^2/V_m)\frac{dr}{dt} \tag{13}$$

The resulting expression for the size dependent rate of the particle radius evolution obtained from eqs 10, 12, and 13 is

$$\frac{dr}{dt} = V_m D C^0_{flat}\left\{\frac{\frac{[M]_{bulk}}{C^0_{flat}} - \exp\left[\frac{2\gamma V_m}{rRT}\right]}{r + \frac{D}{k_g^{flat}}\exp\left[\alpha\frac{2\gamma V_m}{rRT}\right]}\right\} \tag{14}$$

or

$$\frac{dr^*}{d\tau} = \frac{S - \exp\left[\frac{1}{r^*}\right]}{r^* + K\exp\left[\frac{\alpha}{r^*}\right]} \tag{15}$$

The parameters of eq 15, which will be further used in our simulations, are

$$\text{dimensionless radius } r^* = \frac{RT}{2\gamma V_m} r \tag{16}$$

$$\text{dimensionless time } \tau = \frac{R^2T^2DC^0_{flat}}{4\gamma^2 V_m} t \tag{17}$$

$$K = \frac{RT}{2\gamma V_m}\frac{D}{k_g^{flat}} \tag{18}$$

$$S = [M]_{bulk}/C^0_{flat} \tag{19}$$

K is a dimensionless parameter describing the type of the control of the process (the ratio between diffusion and reaction rate constants for a flat interface); S is a dimensionless parameter describing the oversaturation of the monomer in solution.

In the case of pure diffusion control, i.e., when $D \ll k_g^{flat}$ ($K \rightarrow 0$) and $r^* \gg 1$, eq 14 can be simplified to the equation obtained by Sugimoto[19] and applied by Peng[17] to explain of the experimentally observed "focusing" and "defocusing" of the size distributions of growing II−VI and III−V semiconductor NPs:

$$\frac{dr}{dt} = \frac{2\gamma D V_m^2 C^0_{flat}}{rRT}\left(\frac{1}{r_{cr}} - \frac{1}{r}\right) \tag{20}$$

At "critical" radius r_{cr} the rate of dissolution is equal to the growth rate and the size of the NP is time-independent.

3. Simulation of the Ensemble of NPs

In section 2 we described the size evolution of a single NP placed into an infinite volume of solution with fixed monomer concentration. As discussed in the Introduction, there is no general analytical solution describing all processes occurring during the evolution of the entire NP ensemble. For this reason, a Monte Carlo simulation was applied to obtain statistical information about the ensemble behavior. Monte Carlo modeling of the NP ensemble was rather straightforward and similar to those reported in refs 25 and 31. We simulated a volume of 3×10^{-12} cm^3 of the colloidal solution containing 5×10^{3}−5×10^{4} NPs which is in reasonable agreement with the experimental conditions.[7,8,10] The numerical parameters used in the simulation procedure are presented in Table 1.

The evolution of each NP is described by eq 15. The volume fraction of the NPs for all growth stages was below 10^{-3}, so that no correction on the local particle surrounding was necessary.[23] The remaining concentration of monomer and value of the monomer oversaturation S in the solution were calculated after each time step and were substituted into eq 15 to calculate the growth/dissolution rates of the next step. Different statistical parameters (oversaturation of monomer, NP concentration, mean particle size, standard deviation, the shape of size distribution, etc.) were monitored after each time step. The number of NPs used in the simulation allowed to achieve appropriate error values for all statistical parameters.

Two different starting points were used for the simulations performed. In the first approach we considered the nucleation of NPs from an initially homogeneous solution containing a known concentration of monomer. We assumed that the NP nuclei appear in the solution with the rate described by the following equations:[35]

$$J_N = B_N \exp\left(-\frac{\Delta G^N}{RT}\right) \tag{21}$$

$$\Delta G^N = \frac{16\pi\gamma^3 V_m^2}{3(RT\ln S)^2} \tag{22}$$

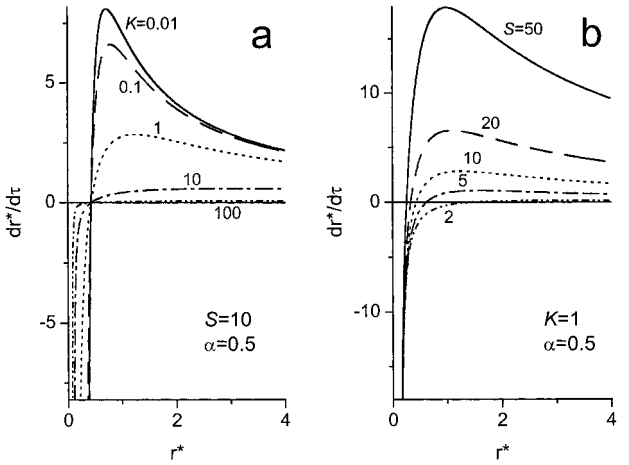

Figure 2. Growth rate vs NP radius calculated from eq 15 for a single NP for different kinds of the kinetics control described by parameter K (a) and for different values of oversaturation S of the monomer (b).

where ΔG^N is the activation energy for homogeneous nucleation; B_N is the preexponential factor depending on many parameters, such as desolvation of species, etc.

In the second approach we simulated experimental conditions where the processes of nucleation and NP growth are completely separated. This situation is realized, e.g., in a so-called "hot-injection" technique of the NP synthesis,[7] when the precursors (monomer) are injected into very hot solvent leading to explosive-like nucleation with a subsequent growth of NPs at lower temperature. In this case the simulation procedure can be started from a preformed ensemble of NPs with some known mean size and Gaussian particle size distribution, and do not take into account the nucleation of new nanocrystals during further growth. This approach does not require the knowledge of the precise kinetics of nucleation.

As no detailed information on the nucleation kinetics in colloidal solutions of real semiconductor NPs is available to date, the simulation of the growth dynamics which involves the above nucleation step might appear rather speculative. However, our calculations show that the influence of the initial conditions is negligibly small and does not affect further evolution of the NP ensemble if the rate of nucleation is much higher than the NP growth rate. This is in accord with the LSW theory predicting a unique shape of the particle size distribution for late stages of growth, being independent of the initial conditions.[21]

4. Results and Discussion

4.1. Growth of a Single NP. The growth rate of a single NP depends strongly on its radius and on the concentration of monomer in solution close to the NP surface. The ratio of reaction and diffusion control is described by the dimensionless parameter K (eq 18). Values of $K < 0.01$ correspond to almost purely diffusion-controlled processes whereas values of $K > 10$ refer to reaction-controlled one. In the range $0.01 < K < 10$ mixed control with comparable contributions of the both processes occurs. The size dependencies of the NP growth rate were calculated from eq 15 for different values of K and S and are presented in Figure 2a,b, respectively. A NP having a radius smaller than some critical radius r_{cr} has a negative growth rate, i.e., dissolves. The value of this "critical" radius corresponding to a net growth rate equal to zero can be easily evaluated from eq 15:

$$r_{cr} = \frac{2\gamma V_m}{RT \ln S} \tag{23}$$

and is equal to the critical nucleation radius.[35]

During growth of a NP, some amount of monomer is consumed in the reaction and, in the case of a finite volume of the solution, the bulk concentration of monomer and the value of oversaturation S decreases gradually. This results in the shift of critical radius toward larger NP size, and the growth rate of the NP decreases (Figure 2b).

4.2. Growth of the NP Ensemble. Two different situations can be experimentally realized at initial stages of the NP growth. The first one occurs if almost all monomer has been involved in the nucleation process and nuclei produced are in the equilibrium with monomer. In this case S depends on the NP mean size and can be estimated from eq 23. The NP growth can occur only via the dissolution of small particles which provide the monomer necessary to form larger ones in the ensemble. This is the classic concept of Ostwald ripening. The situation is different if the nucleation is suppressed before major amount of monomer reacts. This case can be experimentally realized either by the rapid injection of monomer with subsequent fast decrease of the temperature ("hot injection" method),[7] or if the nucleation rate J_N described by eq 21 drops much faster than S decreases. In both cases, large amounts of monomer remains in solution and their concentration is much higher than the equilibrium concentration for the nuclei presenting.

4.2.1. Ostwald Ripening of Nanoparticle Ensemble. LSW and the LSW-based modern theories describe the self-consisted behavior of colloidal particles during Ostwald ripening and predict formation of final ensembles with unique asymptotic particle size distributions. Thus, for a diffusion controlled coarsening the existence of a stationary regime was predicted by the LSW theory[21,22] and is characterized by the following parameters:

$$\text{coarsening rate } \upsilon = \frac{d\langle r\rangle^3}{dt} = \frac{8\gamma V_m^2 D C_{flat}^0}{9RT} \tag{24}$$

limiting stationary size distribution

$$W(r/r_{cr}) = W(u) = \begin{cases} (3^4 e/2^{5/3}) u^2 \exp[-1/(1-2u/3)]/ \\ \qquad [(u+3)^{7/3}(1.5-u)^{11/3}] & \text{if } 0 < u < 1.5 \\ 0 & \text{otherwise} \end{cases} \tag{25}$$

with a cutoff at $u = 1.5$. A particular feature of this LSW distribution is that $\langle r\rangle = r_{cr}$.

For the reaction-controlled coarsening, the equation describing an approximate stationary particle size distribution was obtained by Wagner:[22]

$$W(u) = \begin{cases} 2^7 3u(2-u)^{-5} \exp[-3u/(2-u)] & \text{if } 0 < u < 2 \\ 0 & \text{otherwise} \end{cases} \tag{26}$$

where $\langle r\rangle = 8r_{cr}/9$.

As was mentioned above, the expansion of the Gibbs−Thompson equation used in LSW and other theories is nonvalid for nanoscale systems where terms of higher order begin to play an increasingly important role with decreasing NP size. On the other hand, the Monte Carlo technique allows us to account any particle growth law for the simulation of temporal evolution of the NP ensemble. To study the NP growth under the most ideal conditions, we have assumed complete separation of

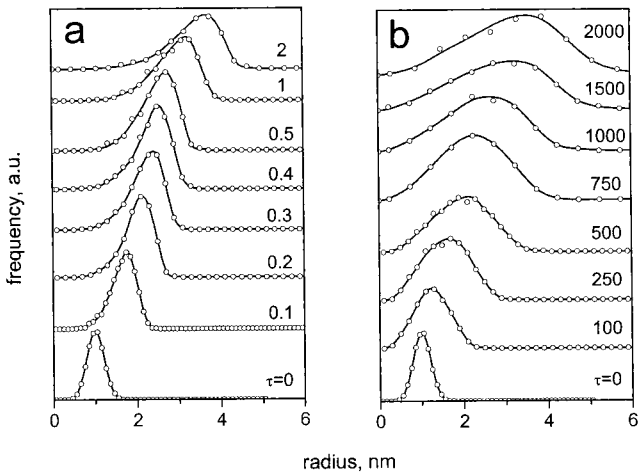

Figure 3. Temporal evolution of size distribution of the NP ensemble during the Ostwald ripening under (a) diffusion ($K = 10^{-3}$) and (b) reaction ($K = 10^{3}$) control.

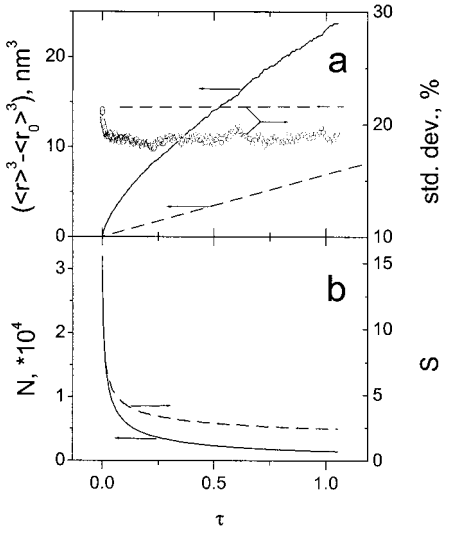

Figure 4. Diffusion-controlled Ostwald ripening ($S_0 = 15$, $K = 10^{-3}$) of the NP ensemble. (a) Evolution of the mean particle radius and standard deviation of particle size distribution in time. Dashed lines correspond to LSW predicted ripening. (b) Change of the number of particles (N) and monomer oversaturation (S) during the ensemble evolution.

nucleation and NP growth, which can be realized, e.g., by the "hot injection" method.[7] The characteristics of the starting NP ensemble (mean radius of NPs 1.0 nm with standard deviation of 20%) used for the simulation were similar to the ones experimentally observed in the synthesis of CdSe nanocrystals from organometallic precursors at 360 °C.[17] An ensemble with similar parameters also forms at initial stages of the synthesis of CdTe nanocrystals in aqueous medium.[37]

Figure 3a shows temporal evolution of the particle size distribution during diffusion-controlled Ostwald ripening ($K = 0.001$). It is clearly seen that initially symmetric normal particle radius distribution evolves in time toward the asymmetric negatively skived one. Similar results were obtained when we varied the standard deviation of the initial normal distribution or even used nonGaussian, e.g., log−normal distributions. After a rather short transient period where the drastic changes in shape of the size distribution occurred, only minor changes were evidenced for later stages of the NP growth. A set of size distribution curves calculated at different instants of time during the reaction-controlled Ostwald ripening ($K = 1000$) is presented in Figure 3b. In the case of reaction-controlled coarsening the particle size distributions were systematically broader as compared to those observed for diffusion-controlled growth. This observation can be explained with the size dependence of the NP growth rate presented in Figure 2a. The difference between r_{cr} and the radius of NP with maximal growth rate (r_{max}) increases gradually with K. Particles smaller than r_{cr} dissolve rapidly, at the same time particles larger than r_{max} have growth rates decreasing with r, and thus, their size distribution narrows down in time.

The temporal evolution of the mean particle radius $\langle r\rangle$ and the standard deviation σ (in %) of the particle size distribution are presented in Figure 4a. The $\langle r\rangle^3$ *vs* τ curve shows a nonlinear behavior during the particle growth in the whole studied range of $\langle r\rangle$ (1.0−3.0 nm), and the growth rate is much higher compared to that predicted by the LSW theory (Figure 4a). This is a result of both the nonstationary regime of coarsening and intrinsic nonvalidity of eq 24 for the nanoscale systems. The value of σ (%) tends to a steady-state value of 18.7 ± 1.0% after a short transient behavior being strongly dependent on the initial conditions. The temporal changes of the oversaturation S and the particle concentration N are presented in Figure 4b. It is worth to mention that the temporal behavior of both S and N is very difficult to determine experimentally with reasonable accuracy.

To simulate Ostwald ripening under different contributions of diffusion and surface reaction, we varied the coefficient K in eq 18. For all values of K tested, the initial standard deviation of particle size distribution (20%) changed drastically during initial stages of the nanocrystals growth. This transient behavior depended strongly on the parameters of the initial particle size distribution. After an increase of the mean radius from 1.0 nm (starting value) to ca. 1.5 nm, some saturation level of σ(%) was reached which was rather stable during further growth, especially in the case of small and large values of K ($K < 0.1$ or $K > 1$). The value of σ corresponding to the saturation level was strongly dependent on K, from 18% for $K < 0.01$ to 35% for $K > 100$. When the regime of the stationary growth was attended, the further coarsening became self-similar with very slow change of the shape of distribution curve keeping σ almost constant. Figure 5 shows nearly stationary particle size distribution curves observed at later stages of Ostwald ripening under different contributions of diffusion and surface reaction as expressed by the coefficient K. The most pronounced difference was observed for $0.01 < K < 10$, whereas below and above this range the influence of K on the shape of the $\sigma(\%)$ vs $\langle r\rangle$ curve was minimal.

The limiting size distributions predicted by the LSW theory for the pure diffusion-limited and reaction-limited cases are shown as dashed lines in Figure 5 for comparison. In the case of diffusion-limited NP coarsening the size distribution is more symmetric and more narrow as compared to the predicted one. Thus, the value of σ inherent to the LSW distribution is ∼21.5%. The simulations of Ostwald ripening of the NP ensembles presented in Figurs 3−5 started from $\sigma = 20\%$ and led to the stationary values of σ of 18 ± 1.5%. This fact is of interest because all previous corrections of the LSW resulted in broadening of the size distributions.[24,27] In fact, many experiments performed for ensembles of large colloidal particles or droplets showed the size distributions being generally broader than predicted by LSW theory for these systems.[27] On the other hand, semiconductor NPs synthesized in colloidal solutions whose growth occurs probably via the Ostwald ripening often showed the particle size distributions markedly below 20%.[7,8,10−12] However, it is worth mentioning that the narrow particle size

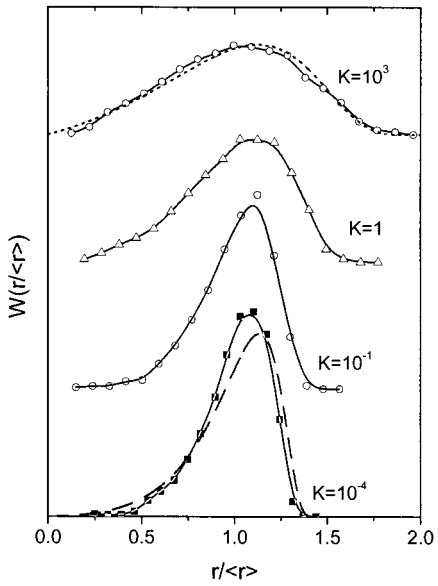

Figure 5. Stationary size distributions observed for the Ostwald ripening of the NP ensemble for different types of kinetics control described by parameter K in eq 15. The limiting distributions predicted by the LSW theory for diffusion- (dashed) and reaction-controlled (dotted) Ostwald ripening are shown for comparison.

distributions observed could be a result of coarsening in a transient regime which will be discussed below.

The most convenient way to present the results of our Monte Carlo simulation for further discussion is a plotting of $\sigma(\%)$ against $\langle r \rangle$. Both parameters can be determined experimentally and allow us to describe the intrinsic statistical behavior of the NP ensemble. Another important point of such presentation is the elimination of the dimensionless time (eq 17), which is the combination of many external parameters such as mass transport coefficient, temperature, etc., and usually is not critical in the NP syntheses.

To ensure that the size distributions narrower than those inherent for the LSW are not a result of the nonstationary transient behavior, we have simulated Ostwald ripening of NPs starting from ensembles with different initial values of σ. The effect of the initial size distribution of NPs on the further evolution of the ensemble is presented in Figure 6a for diffusion-controlled ($K = 0.01$) Ostwald ripening. Almost independent of the initial value of σ, the standard deviation during the NP growth tended asymptotically to the value in the range of 17−20% which is below 21.5% predicted by the LSW. If the initial size distribution was larger than 20%, the Ostwald ripening was accompanied by a "focusing" of the size distribution. This result dispels the conventional statement that Ostwald ripening results only in the broadening of size distributions. The transients from initial size distributions toward the stationary ones accompanied with broadening of the size distributions were much faster than transients accompanied with narrowing of the size distribution (Figure 6a). The simulations started from the very narrow initial size distributions resulted in more smooth and less noisy $\sigma(\%)$ vs $\langle r \rangle$ curves, probably due to the smaller deviations of single particle trajectories during the Monte Carlo simulation route.

The reason why the stationary size distributions of NPs were narrower than predicted by the LSW theory lies, again, in the small radius of NPs. As was mentioned above, the particle growth law used in the LSW assumed $2\gamma V_m/(RT) \ll r$ and higher terms of the expansion of the Gibbs−Thompson equation (eq 1) were omitted. However, if $2\gamma V_m/(RT) \approx r$ or even $> r$,

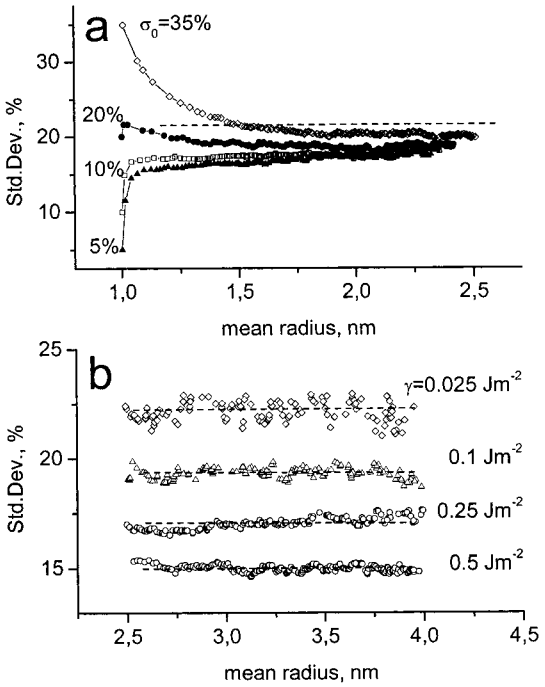

Figure 6. (a) Dependence of the standard deviation of the particle size distribution on the mean particle size during the Ostwald ripening for different values of initial width of particle size distributions. Horizontal dashed line corresponds to LSW predicted ripening. (b) Dependence of the stationary value of standard deviation of the size distribution on the surface tension for the diffusion-controlled coarsening of the NP ensemble. $S_0 = 15$, $K = 10^{-2}$.

these terms play a major role, accelerating the dissolution of particles with radii less than critical. This also results in acceleration of the coarsening rate, as was shown in Figure 4a.

Another feature of the Ostwald ripening of nanoscale systems which is determined by the higher terms of the expansion of the Gibbs-Thompson equation is the dependence of the stationary standard deviation on the surface tension at the particle-solution interface. Figure 6b shows the stationary parts of $\sigma(\%)$ vs $\langle r \rangle$ curves corresponding to different surface tension values and demonstrates the decrease of the stationary value of standard deviation for the increasing γ in the case of diffusion-controlled NP growth in Ostwald ripening regime. If $2\gamma V_m/(RT)$ is markedly larger than r, a stationary value of σ as small as 15% can be achieved (Figure 6b).

The ratio of $2\gamma V_m/(RT)$ and r decreases during the NP growth, so that σ increases slowly and can achieve the LSW predicted value of 21.5% if the condition $2\gamma V_m/(RT) \ll r$ is satisfied at very late stages of particle coarsening. Under the realistic experimental conditions, the mean size of NPs is usually tunable not more than by a factor of 3−4. In this case the ratio between $2\gamma V_m/(RT)$ and r, and as a result, the stationary value of σ remains nearly constant. The similar behavior was observed also for the reaction-controlled NP growth and for the mixed-controlled one.

Summarizing, our simulations show that Ostwald ripening in NP ensembles occurs faster and can result in narrower size distributions than in ensembles of micrometer-scale particles. The most narrow size distribution are achieved if particle growth takes place under strong diffusion control.

4.2.2. Growth of NPs at High Oversaturation of the Monomer: "Focusing" and "Defocusing" of Particle Size Distribution. An interesting transient behavior resulting in strong and fast focusing of the ensemble size distribution can be realized

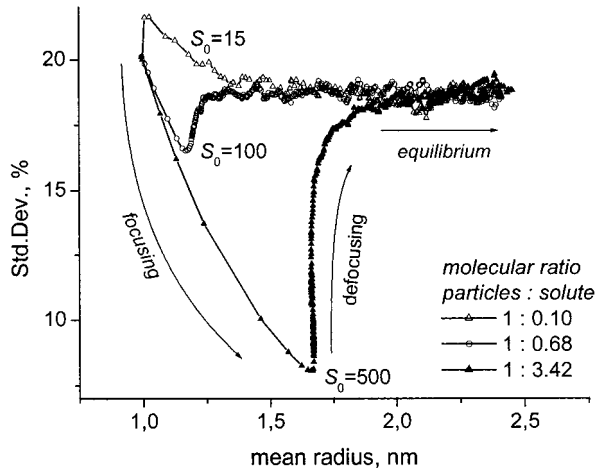

Figure 7. Dependence of the standard deviation of particle size distribution on the mean particle size for different initial oversaturations of monomer in the solution. Arrows show focusing, defocusing, and equilibrium of the size distribution. $K = 10^{-2}$.

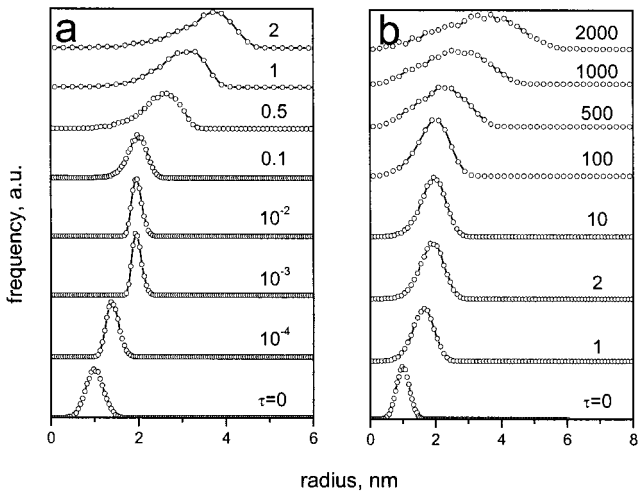

Figure 8. Temporal evolution of the size distribution of the NP ensemble at high initial oversaturation of monomer ($S_0 = 900$) under (a) diffusion ($K = 10^{-3}$) and (b) reaction ($K = 10^{3}$) control.

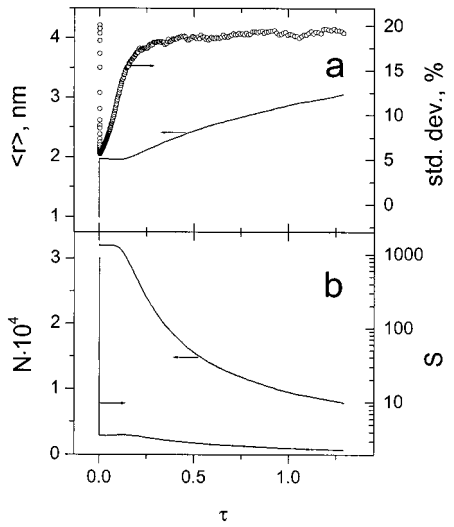

Figure 9. Temporal evolution of the NP ensemble with high initial monomer oversaturation ($S_0 = 900$, $K = 10^{-3}$). (a) Evolution of the mean particle radius and standard deviation of their size distribution in time. (b) Changes of the number of particles (N) and monomer oversaturation (S) during the ensemble evolution.

if the solution initially contains comparatively large amount of monomer. To treat this situation we simulated evolution of NP ensembles with high initial oversaturations, where almost all particles were larger than r_{cr}. Figure 7 shows $\sigma(\%)$ vs $\langle r \rangle$ curves for the diffusion-controlled growth with different initial oversaturations S. The excess of monomer affected strongly the evolution of the size distribution during the initial stages of NP growth. A fast increase of $\langle r \rangle$ accompanied by a strong narrowing of the size distribution is observed, followed by subsequent broadening almost without changes in $\langle r \rangle$ (Figure 7). The position and depth of the minimum of $\sigma(\%)$ depends on the initial oversaturation of monomer. The reaction conditions influencing this parameter can be optimized to produce NPs of desirable size with very narrow size distributions. The temporal evolutions of shape of the size distribution in ensemble of growing NPs are shown in Figures 8a and 8b for the diffusion-controlled and reaction-controlled growth, respectively. In both cases a stable growth regime, more than 10^2 times longer than the previous stage of rapid particle growth, with slow broadening of the particle size distribution at the mean particle size being kept nearly constant was observed. For diffusion-controlled growth the mean radius $\langle r \rangle$ and $\sigma(\%)$ change with time as shown in Figure 9a; the evolution of the number of NPs N and the oversaturation S are given in Figure 9b. In all cases, the nanocrystals have initially positive growth rates and smaller nanocrystals grow faster than the larger ones. The number of particles remains nearly constant during the stage of "focusing" of the size distribution. During the "focusing" stage the size distribution remains nearly symmetric, and it fits well by a normal distribution. The defocusing is accompanied with a transition from symmetric toward asymmetric stationary size distribution. During the focusing stage the oversaturation drops down to some equilibrium value, and the number of nanocrystals starts to decrease due to the dissolution of smallest particles. The Ostwald ripening mechanism governs the further evolution of the NP ensemble.

5. Summary and Outlook

The model has been developed for the evolution of a single NP taking in to account the size dependence of the activation energies of the growth and dissolution processes as well as the mass transport of monomer toward the particle surface. The performed Monte Carlo simulations of the evolution of an ensemble of growing NPs allowed to establish conditions leading to either "focusing" or "defocusing" of the particle size distribution. The stationary particle size distribution inherent to the Ostwald ripening process in ensembles of NPs is narrower and more symmetric than that predicted by the LSW theory. The growth of NPs in the diffusion-controlled regime results in better final size distributions as compared with those grown in the reaction-controlled regime.

We hope that the results of our calculations provide a deeper insight into the processes occurring in the colloidal solutions during the growth of NPs. Of course, the behavior of the real NPs in colloidal solutions may differ from the idealized model we used in this paper, e.g., because of the masking the simple statistics by chemical processes which were outside of our consideration. However, the model may allow the optimization of synthetic routes toward monodisperse NP colloids. Two general strategies to improve the NP size distributions may be proposed. The first is to carry out the process of the NP growth in the diffusion controlled regime, presumably by decreasing the diffusion or mass transfer coefficient of the system. The

second is to increase the surface tension at the solvent−NP interface, for example, by a proper choice of surfactants.

The approach presented here for description of the colloidal solution of NPs might be quite universal and can be applied to different processes occurring via the Ostwald ripening mechanism, e.g., growth of ionic salt crystals, ripening of deposits, etc. As the coarsening processes play an important role in any first-order phase transitions,[38] the deviations from the classical description inherent for the NPs shown in this paper may have to be taken into account for the description of any phase transitions in the nanoscale systems.

Acknowledgment. We thank Dr. A. Eychmüller and Prof. Dr. V. V. Sviridov for stimulating discussions. This work was supported in part by the research projects BMBF-Philips and SFB 508.

References and Notes

(1) For reviews, see: Brus, L. E. *Appl. Phys. A* **1991**, *53*, 465. Banyai, L.; Koch, S. W. *Semiconductor Quantum Dots*; World Scientific: Singapore, 1993. Weller, H. *Angew. Chem., Int. Ed. Engl.* **1993**, *32*, 41. Weller, H. *Adv. Mater.* **1993**, *5*, 88. Alivisatos, A. P. *J. Phys. Chem.* **1996**, *100*, 13226. Nalwa, H. S., Ed. *Handbook of Nanoctructured Materials and Nanotechnology*; Academic Press: New York, 2000. Murray, C. B.; Kagan, C. R.; Bawendi, M. G. *Annu. Rev. Mater. Sci.* **2000**, *30*, 545.

(2) Colvin, V. L.; Schlamp, M. C.; Alivisatos, A. P. *Nature* **1994**, *370*, 354.

(3) Schlamp, M. C.; Peng, X.; Alivisatos, A. P. *J. Appl. Phys.* **1997**, *82*, 5837.

(4) Gao, M.; Lesser, C.; Kirstein, S.; Möhwald, H.; Rogach, A. L.; Weller, H. *J. Appl. Phys.* **2000**, *87*, 2297.

(5) Bruchez, M. P.; Moronne, M.; Gin, P.; Weiss, S.; Alivisatos, A. P. *Science* **1998**, *281*, 2013.

(6) Chan, W. C. W.; Nie, S. *Science* **1998**, *281*, 2016.

(7) Murray, C. B.; Norris, D. J.; Bawendi, M. G. *J. Am. Chem. Soc.* **1993**, *115*, 8706.

(8) Vossmeyer, T.; Katsikas, L.; Giersig, M.; Popovic, I. G.; Diesner, K.; Chemseddine, A.; Eychmüller, A.; Weller, H. *J. Phys. Chem.* **1994**, *98*, 7665.

(9) Micic, O. L.; Curtis, C. J.; Jones, K. M.; Sprague, J. R.; Nozik, A. J. *J. Phys. Chem.* **1994**, *98*, 4966.

(10) Gao, M.; Kirstein, S.; Möhwald, H.; Rogach, A. L.; Kornowski, A.; Eychmüller, A.; Weller, H. *J. Phys. Chem. B* **1998**, *102*, 8360.

(11) Talapin, D. V.; Rogach, A. L.; Kornowski, A.; Haase, M.; Weller, H. *Nano Lett.* **2001**, *1*, 207.

(12) Talapin, D. V.; Haubold, S.; Rogach, A. L.; Kornowski, A.; Haase, M.; Weller, H. *J. Phys. Chem. B* **2001**, *105*, 2260.

(13) Eychmüller, A. *J. Phys. Chem. B* **2000**, *104*, 6514.

(14) Woggon, U. *Optical Properties of Semiconductor Quantum Dots*; Springer-Verlag: Berlin, 1997.

(15) Gaponenko, S. V. *Optical Properties of Semiconductor Nanocrystals*; Cambridge University Press: Cambridge, 1998.

(16) Empedocles, E. A.; Neuhauser, R.; Shimizu, K.; Bawendi, M. G. *Adv. Mater.* **1999**, *11*, 1243.

(17) Peng, X.; Wickham, J.; Alivisatos, A. P. *J. Am. Chem. Soc.* **1998**, *120*, 5343.

(18) Peng, Z. A.; Peng, X. *J. Am. Chem. Soc.* **2001**, *123*, 1389.

(19) Sugimoto, T. *Adv. Colloid Interfac. Sci.* **1987**, *28*, 65.

(20) Ostwald, W. *Z. Phys. Chem.* **1901**, *37*, 385.

(21) Lifshitz, I. M.; Slyozov, V. V. *J. Phys. Chem. Solids* **1961**, *19*, 35.

(22) Wagner, C. *Z. Elektrochem.* **1961**, *65*, 581.

(23) Marqusee, J.; Ross, J. *J. Chem. Phys.* **1984**, *80*, 536.

(24) Voorhees, P. W. *J. Stat. Phys.* **1985**, *38*, 231.

(25) Yao, J. H.; Elder, K. R.; Guo, H.; Grant, M. *Phys. Rev. B* **1993**, *47*, 14110.

(26) Venzl, G. *Phys. Rev. A* **1985**, 31, 3431.

(27) Kabalnov, A. S.; Shchukin, E. D. *Adv. Colloid Interfac. Sci.* **1992**, *38*, 69.

(28) Carlow, G. R.; Zinke-Allmang, M. *Phys. Rev. Lett.* **1997**, *78*, 4601.

(29) De Smet, Y.; Deriemaeker, L.; Parloo, E.; Finsy, R. *Langmuir* **1999**, *15*, 2327.

(30) Egelhaaf, S.; Olsson, U.; Schurtenberger, P.; Morris, J.; Wennerström, H. *Phys. Rev. E* **1999**, *60*, 5681.

(31) De Smet, Y.; Deriemaeker, L.; Finsy, R. *Langmuir* **1997**, *13*, 6884.

(32) Venzl, G. *Ber. Bunsen-Ges. Phys. Chem.* **1983**, *87*, 318.

(33) Yao, J. H.; Elder, K. R.; Guo, H.; Grant, M. *Phys. Rev. B* **1992**, *45*, 8173.

(34) Berry, R. S.; Rice, S. A.; Ross, J. *Physical Chemistry*; Oxford University Press: Oxford, 2000.

(35) Nielsen, A. E. *Kinetics of precipitation*; Oxford. New York, 1964.

(36) Zener, C. *J. Appl. Phys.* **1949**, *20*, 950.

(37) Rogach, A. L.; Katsikas, L.; Kornowski, A.; Su, D.; Eychmüller, A.; Weller, H. *Ber. Bunsen-Ges. Phys. Chem.* **1996**, *100*, 1772.

(38) Marqusee, J.; Ross, J. *J. Chem. Phys.* **1983**, *79*, 373.